Article:
Jindal, G, Watkins, GT, Morris, K orcid.org/0000-0002-0090-9121 et al. (1 more author) (2022) Digital Predistortion of RF Power Amplifiers Robust to a Wide Temperature Range and Varying Peak-to-Average Ratio Signals. IEEE Transactions on Microwave Theory and Techniques, 70 (7). pp. 3675-3687. ISSN 0018-9480

https://doi.org/10.1109/tmtt.2022.3175155

Digital Pre-Distortion of RF Power Amplifiers Robust to a Wide Temperature Range and Varying Peak-to-Average Ratio Signals

Gautam Jindal, *Student Member, IEEE,* Gavin T. Watkins, *Member, IEEE,*
Kevin Morris *Member, IEEE,* and Tommaso A. Cappello, *Member, IEEE*

***Abstract*—In this work, a digital pre-distortion (DPD) model for the linearization of RF power amplifiers (PAs) is presented. The model provides a linearized gain (DPD+PA) independent from the instantaneous transistor channel temperature within a pre-defined temperature window. Channel temperature variations due to varying ambient temperatures or changes in the signal probability density function (PDF) cause long-term memory effects, which results in dispersed (dynamic) AM/AM and AM/PM characteristics. The presented model is used to compensate for the memory effects due to self-heating and external temperature changes by estimating the transistor channel temperature through a linear single-pole Foster thermal network. The DPD model uses a first-order Taylor approximation to cancel out temperature based non-linearities. Gaussian pulses are used to extract the PA intra-pulse gain at different temperatures without being affected by the signal PDF, thus allowing temperature- and signal-independent PA characterization. The model is validated from $20\,^{\circ}$C to $80\,^{\circ}$C and by considering a class-B 3.75-GHz 10-W GaN-on-SiC PA. The DPD performance is evaluated by considering the Normalized Root Mean Square Error (NRMSE), the output spectra, and Adjacent Channel Power Ratio (ACPR) with and without DPD for multiple signals bandwidths and Peak-to-Average Power Ratio (PAPR) and finally compared with other approaches.**

***Index Terms*—behavioural modelling, digital pre-distortion (DPD), Gallium-Nitride (GaN), linearization, memory effects, RF power amplifier, temperature degradation, thermal effects.**

I. Introduction

Typical RF power amplifiers (PAs) can deliver high output powers (>100 W) with peak efficiencies up to 50-70% and of 10-20% at average when signals with high peak-to-average power ratios (PAPRs) are used (i.e. 6 to 12dB) [1]. With such efficiencies, when a signal with amplitude modulation is considered, the time-dependant dissipated power generates heat which causes the PA, and the transistor within it, to operate differently from its iso-thermal[1] characteristics [1]. This temperature-dependent non-linearity creates in-band and out-of-band distortion [2].

Manuscript received XXX, XXX; revised XXXX, XXXX; accepted XXXX, XXXX.

This paper is an expanded version from the 2021 International Microwave Symposium (IMS), Atlanta, GA, USA, June 7–10, 2021. (Corresponding author: Gautam Jindal.)

G. Jindal, K. Morris, and T. A. Cappello are with the Department of Electrical and Electronic Engineering, ,UK, BS8 1UB, e-mail: (gj13100@bristol.ac.uk).
G. Watkins is with Toshiba Research Europe Limited.

[1]For iso-thermal we intend a PA characteristic with no temperature variation.

In a typical PA, the transistor is the most temperature-sensitive component. In high-electron-mobility transistors (HEMTs), the temperature reduces the associated trans-conductance and increases the on-resistance [3], [4]. The thermal diffusion from the transistor channel hot-spot (typically located under the gate) to the environment can be modelled with a Cauer or Foster thermal network [5]. Its thermal impedance is mainly determined by the transistor stack-up geometries and materials (e.g. thickness of the buffer layer), such as the transistor substrate (e.g., Si vs. SiC), carrier (e.g. CuW vs. CuMo) and finally by the attachment to the baseplate (e.g., mechanical vs. solder joint). To ensure adequate cooling to the transistor, heat-sinks, fans, Peltier cells, and/or liquid cooling systems can be used [5]. A well-designed cooling system presents a low thermal impedance to the environment which limits the transistor average temperature for a given lifetime and the transistor peak temperature to avoid thermal breakdown. Reducing the cooling hardware can lessen the weight, size, and power requirements of the overall PA, but it will negatively affect its amplification characteristics as the temperature fluctuation is higher.

In the last two decades, AlGaN/GaN has demonstrated superior RF power-amplification performance as compared to Si and this is due to its large carrier mobility, wide band-gap energy, and high breakdown voltage. This translates into devices with smaller footprints, higher power densities and efficiencies up to mm-waves [6], [7]. GaN has enabled multiple industries to expand with the future of high-frequency RF power amplification to be GaN-based, with a predicted compound annual growth rate (CAGR) of 19.8 % from 2020 to 2027 [**?**]. On the other hand, because of the high power densities, large temperature gradients can develop on the chip making the aforementioned thermal issues more detrimental in GaN than in other technologies. These issues are also magnified by the large temperature window of GaN semiconductors, with examples of transistors operating up to $500\,^{\circ}$C [8]. The heat developed in transistors, in fact, spreads around the whole circuit due to the high thermal conductivity of the substrate (especially with SiC) which degrades the whole circuit performance [9]–[11].

To avoid large temperature variations, the input signal can be altered through crest factor/PAPR reduction techniques. The reduction of the signal's PAPR can lead to less self-heating and higher average output power. However, these PAPR reduction

techniques cause EVM degradation [12] of the original signal. Thus modelling these effects is a more general way of approaching this problem as it is assumed a DPD unit is already present in the baseband.

To measure the transistor temperature, direct and indirect techniques are typically used. Direct techniques are based on infra-red (IR) or Raman spectroscopes to measure the transistor surface temperature. IR techniques are limited in spatial resolution because of the long wavelength [13] of the infra-reds, Raman techniques operate at higher frequencies and so are inherently capable of higher spatial resolutions. [14] demonstrates a Raman setup with a space and time resolution of 0.5-0.7 μm and 200 ns respectively. Both techniques, however, require direct access to the transistor (which is often enclosed in a package), and bulky and expensive illuminators not suitable for use in a base-station environment. Indirect techniques are instead based on the observation of electrical quantities (i.e., RF output voltage or supply current) to predict the temperature from iso-thermal measurements. This approach is only capable to extract a transistor channel temperature with a coarse spatial resolution (because of the temperature sensor size and placement) but with significant time-resolution because of the fast generation/acquisition bandwidths of modern RF instruments. The works [15]–[19] are demonstrations of indirect temperature sensing techniques whereas the knowledge of the internal temperature is used to predict the PA output power in CW and pulsed modes.

One of the applications of PA behavioural modelling is the linearization of RF PAs through digital pre-distortion (DPD) [20]. [21] shows a tuning algorithm that changes the PA bias voltages based on temperature and in joint operation with DPD. [22] uses a custom generalised memory polynomial approach using a residual approximation to extract the physical time constant of self-heating, [23] presents a DPD with a measurement set acquired at a single ambient temperature to compensate a wide range of temperatures. [24] presents an analogue circuit for the compensation of memory effects (including thermal) allowing complexity reduction of DPD.

This work presents a DPD that is robust to varying signal PAPRs (6 to 12 dB) and/or operating temperatures (20 to 80 °C) by using temperature feedback sensing the case temperature of the PA as shown in Fig. 1. It is shown that different signals cause different temperature-related effects, and by employing a simple memory-less iso-thermal characterisation done using single Gaussian pulses instead of actual OFDM or LTE signals and with the additive thermal sensitivity term this DPD is able to correct for the AM/AM and AM/PM alterations due to the heating/cooling PA with a significant memory reduction at the output. We note that this model does not consider any short-term effects and only concentrates on temperature induced effects. With the proposed DPD, a single gain G_{lin} is achieved after the system $PA + DPD$ irrespective of the external temperature variation or variation to the signal PDF. The proposed DPD can dramatically reduce the feedback bandwidth of a real-time system as the case temperature variation varies in the Hz range.

This paper is organized as follows. Section II introduces the DPD model and the relevant design equations. Section III presents the experimental setup with Section IV expressing the PA characterisation for DPD. Section V presents the DPD validation, with emphasis on its robustness to varying PAPRs and external temperatures and finally concluding the findings of this work at the end.

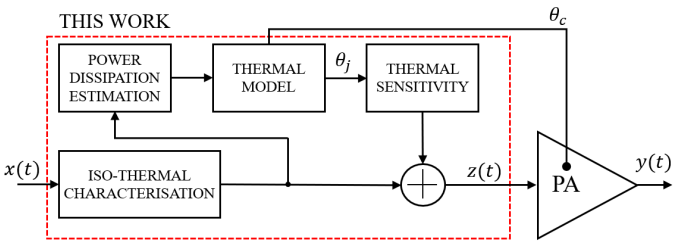

Fig. 1: Block diagram of the presented DPD model. A DPD obtained with pulsed iso-thermal measurements is corrected over an extended temperature range by dynamically calculating the transistor channel temperature (θ_j) starting from a measured case temperature (θ_c) and dissipated power.

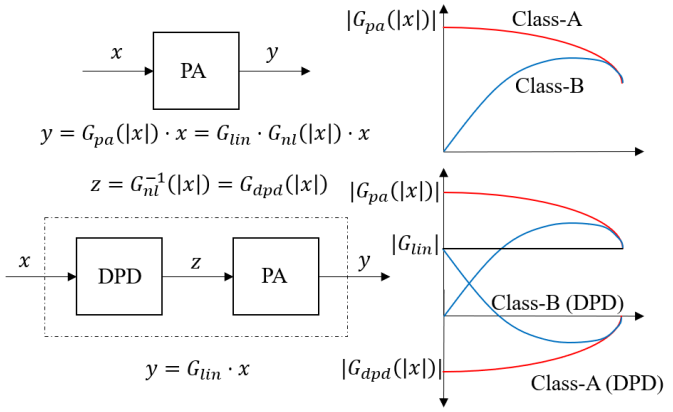

Fig. 2: Top: PA gain model (G_{pa}) and typical gain amplitude characteristics for a class-A and -B PA. Bottom: use of the inverted PA model (G_{dpd}) for linearization purposes for a class-A and -B PA.

II. DPD Model Identification

A. PA Non-linearity Correction with DPD

The baseband-equivalent AM/AM and AM/PM non-linear model of a PA can be expressed as

$$y = G_{pa}(x) = G_{lin} \cdot G_{nl}(x), \tag{1}$$

where x and y are the normalized input and output voltage waves in a 50 Ω environment. The gain G_{pa} is then normalized to 1 by introducing the normalization constant G_{lin} and G_{nl} is the non-linear part of the model. The effect of the non-linearity is depicted in Fig. 2(top) for a class-A and class-B PA.

If the inverse gain function $G_{nl}^{-1}(x)$ exists[2], it is possible to eliminate the nonlinear part by introducing a new signal z such that

$$y = G_{lin} \cdot G_{nl}(z) = G_{lin} \cdot x \quad \rightarrow \quad z = G_{nl}^{-1}(x). \tag{2}$$

The signal z is typically referred to as pre-distorted signal and by using z instead of x, it is possible to achieve linear amplification with a constant gain and phase difference for the

[2]This is typically the case with solid-state PAs.

range specified by the input x. Experimental evidence shows that RF-PAs are only sensitive to the amplitude of x and not to its phase, hence $G_{pa}(x) \cong G_{pa}(|x|)$.

With DPD, the nonlinear inverse function $G_{nl}^{-1}(|x|)$ is implemented digitally, hence it is here called $G_{dpd}(|x|) = G_{nl}^{-1}(|x|)$ and interpreted as the inverse of the non-linear gain. In fact, when $|G_{nl}^{-1}(|x|)|$ is expressed in dB, it can either have positive or negative values depending on the class of operation as shown in Fig. 2(bottom).

B. DPD Modelling With Temperature Effects

Let us now consider a DPD nonlinear gain G_{dpd} with dependence on the PA transistor channel temperature $\theta_j(t)$, namely

$$z(t) = G_{dpd}(|x(t)|, \theta_j(t)). \tag{3}$$

Here, $x(t)$ is the original input signal, $z(t)$ is the pre-distorted signal, and $\theta_j(t)$ is the transistor channel temperature. Along with this model, we introduce the temperature-dependent PA drain current function F_{pa} defined as

$$i(t) = F_{pa}(|x(t)|, \theta_j(t)). \tag{4}$$

In the following, the time-dependency from the variables is removed for brevity.

Assuming the DPD gain and drain current scale linearly with respect to the transistor channel temperature (as shown in [19]), it is possible to linearize (3) around a fixed temperature θ_j^* by considering a Taylor 1^{st} order approximation

$$G_{dpd}(|x|, \theta_j) \cong G_{dpd}(|x|, \theta_j^*) + g_{dpd}(|x|)(\theta_j - \theta_j^*). \tag{5}$$

Similarly, for the PA drain current function (4) results

$$F_{pa}(|x|, \theta_j) \cong F_{pa}(|x|, \theta_j^*) + f_{pa}(|x|)(\theta_j - \theta_j^*). \tag{6}$$

The first terms, $G_{dpd}(|x|, \theta_j^*)$ and $F_{pa}(|x|, \theta_j^*)$, are here called the iso-thermal DPD gain and iso-thermal drain current functions, respectively. As it will be later shown, these functions are representative of the PA characteristics at a single temperature (θ_j^*). The second term in (5)-(6), $g_{dpd}(|x|)$ and $f_{pa}(|x|)$, are the DPD gain thermal sensitivity and drain current thermal sensitivity. These sensitivities are multiplied by the temperature variation in respect to the temperature θ_j^*. These sensitivities are defined as the derivatives of the iso-thermal gain and current with respect to the temperature and can be approximated with the finite difference

$$\begin{aligned} g_{dpd}(|x|) &= \frac{\partial G_{dpd}(|x|, \theta_j^*)}{\partial \theta} \\ &\cong \frac{G_{dpd}(|x|, \theta_j^* + \Delta\theta) - G_{dpd}(|x|, \theta_j^*)}{\Delta\theta}, \\ f_{pa}(|x|) &= \frac{\partial F_{pa}(|x|, \theta_j^*)}{\partial \theta} \\ &\cong \frac{F_{pa}(|x|, \theta_j^* + \Delta\theta) - F_{pa}(|x|, \theta_j^*)}{\Delta\theta}. \end{aligned} \tag{7}$$

Here, $\Delta\theta$ is the channel temperature variation over which the sensitivities are estimated. Because the gain and current scale linearly with temperature in the considered range of 20 °C to 80 °C, $\Delta\theta$ can be chosen arbitrarily large (here is 60 °C).

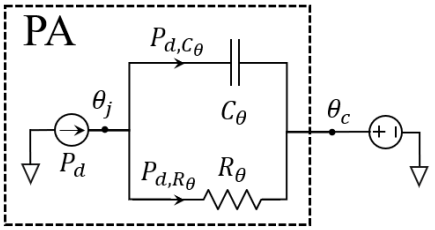

Fig. 3: Single-pole Foster thermal network with thermal resistance R_θ and capacitance C_θ. This network is used to estimate the channel temperature θ_j from a measured case temperature θ_c and dissipated power P_d.

C. PA Thermal Network

Assuming a negligible power is reflected and dissipated by the PA matching and bias networks, the dissipated power $P_d(t)$ in the transistor can be estimated by

$$P_d(t) \cong |x(t)|^2 + V_{ds} \cdot i(t) - |y(t)|^2, \tag{8}$$

where $P_i = |x(t)|^2$ is the RF input power, $P_o = |y(t)|^2$ is the RF output power, V_{ds} is the drain supply voltage, and $V_{ds} \cdot i(t)$ is the drain power consumption of the PA.

The PA thermal network is modelled using a thermal-electrical equivalent circuit (Foster model). A single-pole network is found to be sufficient for this work [25] and its schematic is shown in Fig. 3 . The thermal resistance R_θ and capacitance C_θ are used to model the temperature difference between the channel and case. In this Foster model, $P_d(t)$ acts as a current source whose value can be expanded as

$$P_d(t) = P_{d,R_\theta}(t) + P_{d,C_\theta}(t), \tag{9}$$

where $P_{d,R_\theta}(t)$ and $P_{d,C_\theta}(t)$ are the currents flowing through the resistor R_θ and through the capacitor C_θ, respectively.

By defining $\theta_{jc}(t) = \theta_j(t) - \theta_c(t)$, it follows

$$P_{d,R_\theta}(t) = \frac{\theta_{jc}(t)}{R_\theta}, \quad P_{d,C_\theta}(t) = C_\theta \frac{\mathrm{d}\theta_{jc}(t)}{\mathrm{d}t}, \tag{10}$$

Substituting (10) in (9), it results in the first-order differential equation

$$P_d(t) = \frac{\theta_{jc}(t)}{R_\theta} + C_\theta \frac{\mathrm{d}\theta_{jc}(t)}{\mathrm{d}t}. \tag{11}$$

This last equation needs to be discretized in the time domain in order to be evaluated by a PC. To this aim, we consider a sampling time $\Delta t = 4$ ns much smaller than the fastest time constant of the system $R_\theta C_\theta = 3.5$ ms. The derivative in (11) can be approximated using the finite difference, hence

$$\frac{P_d(t)}{C_\theta} \cong \frac{\theta_{jc}(t)}{C_\theta R_\theta} + \frac{\theta_{jc}(t + \Delta t) - \theta_{jc}(t)}{\Delta t}, \tag{12}$$

and after rearranging, it follows

$$\theta_{jc}(t + \Delta t) = \left(1 - \frac{\Delta t}{R_\theta C_\theta}\right)\theta_{jc}(t) + \frac{\Delta t}{C_\theta} P_d(t). \tag{13}$$

From this, the channel temperature can be computed as $\theta_j(t) = \theta_{jc}(t) + \theta_c(t)$. We note that $\theta_c(t)$ is known as it is measured on the PA case with a temperature sensor. This thermal network has proven to be sufficient to capture the self-heating effects as later shown.

D. DPD Model Extraction

Because of the DPD nonlinearity, the pre-distorted signal $z(t)$ presents new frequency components compared to the original signal $x(t)$. In this experimental setup an $f_s = 1/T = 250\,\text{MHz}$ is used to capture the signals including also distortion. Assuming to sample at intervals $t = nT$ with $n = 1, 2, 3, ...$, the signals $[x(t), y(t), z(t), i(t)]$ are represented by the samples $[x(n), y(n), z(n), i(n)]$ and so they can be captured with a time-sampling system (VSG/VSA and an oscilloscope). The DPD function G_{dpd} can thus be identified with measurements during a preliminary PA characterization phase by swapping the PA input with the output.

The digital gain G_{dpd} can now be evaluated for an arbitrary signal by using linear interpolation or by least-square fitting it to a function, such as a polynomial, and this is the approach used in the following,

$$G_{dpd}(|x(n)|, \theta_j^*) = \sum_{k=0}^{K_G} \gamma_k(\theta_j^*)|x(n)|^k. \tag{14}$$

In this equation, K_G is the polynomial order[3] and $\gamma_k(\theta_j^*)$ are the DPD polynomial coefficients for the PA at the channel temperature θ_j^*.

When (14) is obtained for two temperatures separated by $\Delta\theta$, the DPD thermal sensitivity function can be calculated as the difference of the polynomial coefficients at two temperatures, separated by $\Delta\theta$

$$g_{dpd}(|x(n)|) = \frac{\sum_{k=0}^{K_G}\left[\gamma_k(\theta_j^* + \Delta\theta) - \gamma_k(\theta_j^*)\right]|x(n)|^k}{\Delta\theta}. \tag{15}$$

Next, the iso-thermal drain current function is fitted to a polynomial, hence

$$F_{pa}(|x(n)|, \theta_j^*) = \sum_{k=0}^{K_F} \phi_k(\theta_j^*)|x(n)|^k. \tag{16}$$

Here, K_F is the polynomial order and $\phi_k(\theta_j^*)$ are the polynomial coefficients of the PA at the temperature θ_j^*. Same consideration as for the DPD gain applies for calculating the thermal sensitivities of the drain current,

$$f_{pa}(|x(n)|) = \frac{\sum_{k=0}^{K_F}\left[\phi_k(\theta_j^* + \Delta\theta) - \phi_k(\theta_j^*)\right]|x(n)|^k}{\Delta\theta}. \tag{17}$$

In conclusion, the inverted model for DPD correction using a linearized temperature dependence is here summarized as

$$\begin{cases} z(n) = G_{dpd}(|x(n)|, \theta_j^*) + g_{dpd}(|x(n)|)(\theta_j(n) - \theta_j^*), \\ i(n) = F_{pa}(|x(n)|, \theta_j^*) + f_{pa}(|x(n)|)(\theta_j(n) - \theta_j^*), \\ P_d(n) = |x(n)|^2 + V_{ds} \cdot i(n) - |y(n)|^2, \\ \theta_j(n) = \theta_{jc}(n) + \theta_c(n), \\ \theta_{jc}(n) = \left(1 - \frac{\Delta t}{R_\theta C_\theta}\right)\theta_{jc}(n-1) + \frac{\Delta t}{C_\theta} P_d(n-1), \end{cases} \tag{18}$$

where G_{dpd}, g_{dpd}, F_{pa}, and f_{pa} polynomial models can be calculated using (14)-(17).

[3]The order of the polynomial is selected to be the lowest necessary to minimize the root mean square error between the polynomial model and the measured data without over-fitting.

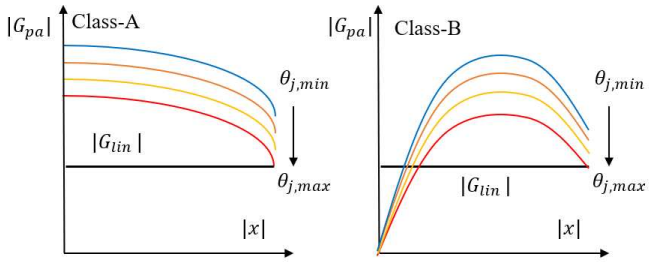

Fig. 4: Qualitative PA iso-thermal characteristics for a class-A or -B PA showing the normalization of the large-signal gain of the device to the highest temperature considered in the operating window $[\theta_{j,min}, \theta_{j,max}]$. Higher linearized gains G_{lin} can be obtained by narrowing the temperature window to lower temperatures.

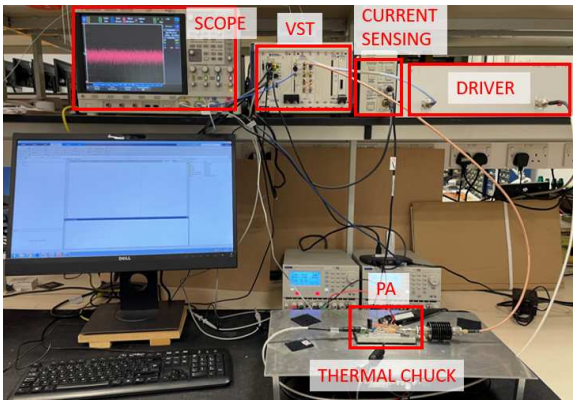

Fig. 5: Picture of the setup created for this work.

An essential requirement of this model is to achieve linear operation ($y = G_{lin} \cdot x$) independently from self-heating effects or external temperature variations. In MOSFET-like transistors, the gain at large signal reduces with increasing temperatures. This concept is qualitatively depicted in Fig. 4 for a class-A or -B PA. When a temperature window from $\theta_{j,min}$ to $\theta_{j,max}$ is considered, the maximum achievable PA gain is $G_{pa}(|x|_{max}, \theta_{j,max})$. When linearization to the peak power is considered, the linearized gain is $G_{lin} = G_{pa}(|x|_{max}, \theta_{j,max})$, as also shown in Fig. 4. Lower gain values can also be selected but at the expense of a reduced PA efficiency. Extending the temperature window to higher temperatures results in a lower linearized gain G_{lin}. This issue can be mitigated by selecting a transistor with a large-signal gain less sensitive to temperature.

Regarding the thermal part of the model, the recursive formula containing θ_{jc} requires initialization. In the considered case of a class-B amplifier, this is $\theta_{jc}(0) = 0\,^\circ\text{C}$ because $P_d(0) \cong 0\,\text{W}$ for $t \leq 0$. If the PA is biased ($i(t) \neq 0$ for $t \leq 0$), it is necessary to consider the self-heating due to the quiescent current, hence, $\theta_{jc}(0) = R_\theta P_d(0)$ with $P_d(0) = V_{dc} i(0)$.

III. Experimental Setup

For the validation, the setup of Fig. 5 is created around an in-house designed and fabricated 3.75-GHz PA based on a 10-W GaN-on-SiC HEMT (Wolfspeed CG2H40010F). The PA is biased in class-B with supply voltage $V_{ds} = 28\,\text{V}$ and $i_q = 0\,\text{mA}$ at room temperature and provides 10 dB gain, 50 %

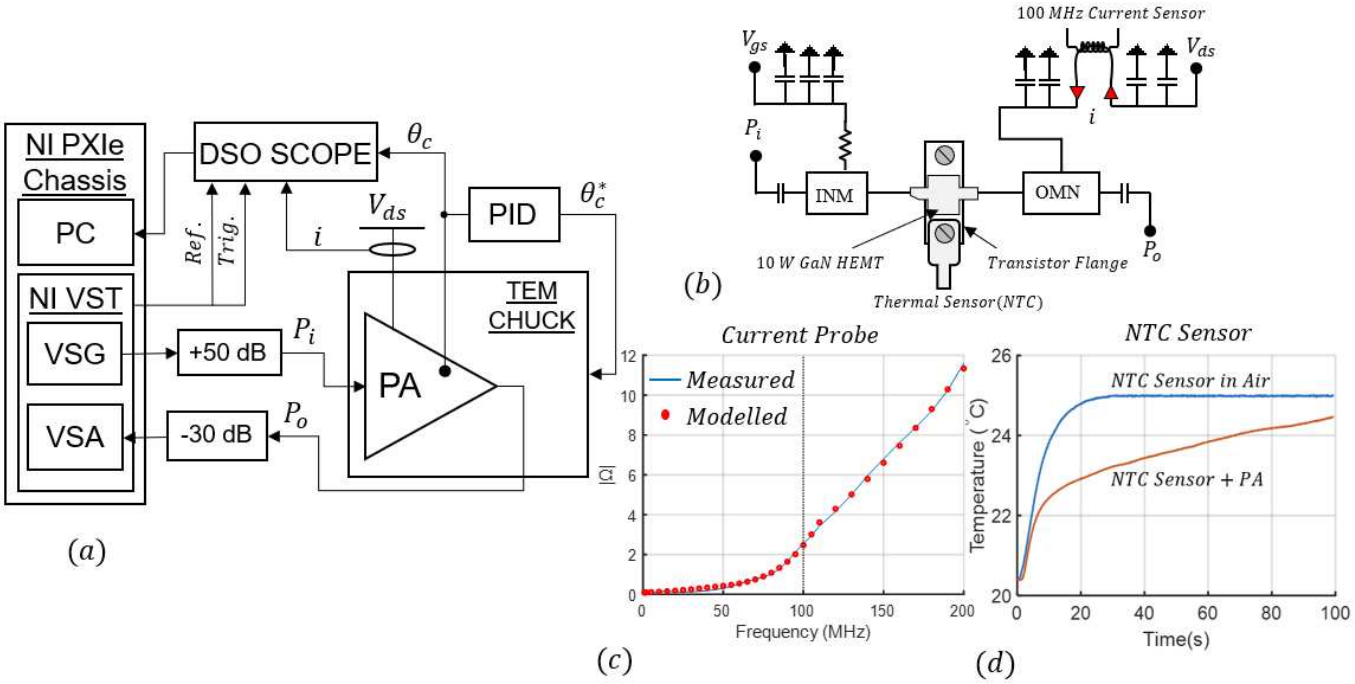

Fig. 6: (a): Block diagram of the custom setup created around a 10W GaN HEMT based PA, capable to acquire all electrical quantities $(P_i, P_o, V_{ds}, i, \theta_c)$ for temperature based DPD. (b): Block diagram of the PA circuit with attached NTC thermal sensor to the flange of the packaged transistor and 100 MHz current sensor clamped to a custom drain line fabricated in between the RF and DC bypass capacitors. (c): Impedance of the current probe, measured and the modelled values. The modelled values are used to evaluate the PA performance with the probe attached. (d): Measured and modelled step response of the thermal sensor for a 100-s stimulus, plotted on the time-based scale for when in air and when it is connected to the flange.

peak Power Added Efficiency (PAE) at $P_i = 32\,dBm$ when the channel temperature is $\theta_j = 80\,°$C.

To extract the PA's characteristics at different temperatures, the PA is mounted on a Thermo-Electrical-Module (TEM) chuck (Laird Power Cool DA-075-24-02), in Fig. 6(a), and thermal grease is applied to make a strong thermal contact between the PA baseplate and chuck. The chuck can regulate and stabilise different case temperatures (θ_C^*), in this case between $20°-$ and $80°$C, using a Proportional-Integrative-Derivative (PID), tuned using the Ziegler-Nichols method, to achieve a fast settling time with low steady-state error. To have knowledge of the case (flange) temperature that is to be used for further temperature estimation, the transistor in the PA is bolted down to the baseplate with a Negative Thermal Coefficient (NTC) sensor (Vishay NTCALUG03A), Fig. 6(b). This NTC sensor is well connected with the flange of the HEMT, which in this case is the closest contact that can be made for thermal analysis without altering the packaged transistor.

In terms of RF input generation and output acquisition, the PA is connected to a 200-MHz vector signal transceiver (National Instruments VST PXIe-5646R) which is controlled by a PC embedded in a NI rack. Between that, a driver (Empower 1178BBM58CGM) providing 50-dB linear gain is used at the input and a 30-dB attenuator is connected to the PA output. Calibration is performed with a power meter at the PA reference planes.

The PA drain current $i(t)$ is measured using a current clamp (Tektronic TCPA312) with an AC+DC instantaneous bandwidth of 100 MHz. The sensor is clamped around a wire loop, the ends of which are connected to a slot fabricated in the drain feed line between the PA RF bypass capacitors and DC bypass capacitors, in Fig. 6(b). Introducing the current clamp with the alteration of the drain line was first modelled in Keysight's Advanced Design System (ADS) to ensure no changes are observed in the PA's intrinsic characteristics. For this, the impedance of the wire loop+current clamp are measured and then simulated in ADS to come up with the appropriate location for this alteration in the bias network. As it can be noticed from Fig. 6(c), the impedance is negligible in the considered bandwidth (10-20 MHz LTE), also after allowing 3-4 oversampling for PA nonlinearity. This measurement confirms the possibility of acquiring real-time current without affecting normal PA operation.

The output of the current clamp is connected to a 12-bit oscilloscope (Keysight DSO-9094A), triggered and connected with a 10-MHz reference from the VST for real-time acquisition. The voltage of the NTC sensor is measured by the oscilloscope and its value is sensitive to temperature variations with a negative thermal coefficient. The manufacturer-provided Steinhart-Hart coefficients are used to convert this voltage into a temperature in degree Celsius.

To verify that the temperature sensor bandwidth is enough to capture the temperature variation at the transistor case, the step response of the NTC sensor in air and attached to the transistor case is reported in Fig. 6(d). For this, a 100-s heat step is applied to the sensor, at the ambient temperature of 20.4 °C, first in air and then attached to the transistor case. When the sensor is in the air, its response can be estimated as a first-order exponential with a time constant of 6.1 s. When

the sensor is attached to the PA flange, this response becomes slower as a consequence of the added junction-case thermal capacitance C_θ. Therefore this temperature sensor is adequate for capturing such a slow temperature variation.

We also note this low-frequency signal with an estimated bandwidth of at least 1/6.1 s = 164 mHz needs to be acquired by the digital baseband for use in this DPD. This low-frequency signal can be used as in feedback for the model, without needing coefficient updates through power-hungry and expensive downconverters + ADCs as in other common approaches (e.g. feedback with coefficient update).

IV. PA Characterization for DPD

A. Gaussian Pulse Characterization

Complex signals such as LTE, when amplified in a GaN transistor, can induce a large temperature variation between the channel and the outside ambient [25]. Due to the physical structure of these GaN HEMTs, the rise of the channel temperature is low-pass filtered by the thermal network [26]. In wide-band signals such as OFDM with MHz bandwidth, the channel temperature follows the filtered, average, value of the dissipation in the transistor [25].

To develop a temperature-sensitive DPD, the PA needs to be characterised at different temperatures. If an actual OFDM or LTE signal is used for this, the temperature effects embedded in the DPD coefficients are only efficient for that specific dissipation profile. These DPD coefficients if used for a different signal will not provide adequate linearization and this is experimentally demonstrated later. For a complete thermal characterisation using actual communication signals, multiple signal types with varying PAPRs would be required. This would increase the complexity of the characterisation and require a greater FPGA memory where the information of this characterisation would be held in terms of coefficients [27]. At last, for such a linearization process, prior knowledge of the input signal would be necessary for the pre-distorter to switch between the different characterisations.

A new characterization technique is thus required with the goal of capturing the PA characteristics at different temperatures independently from the dissipated power. From [28], it is possible to decompose an OFDM signal using a single Gaussian pulse, with duration inversely proportional to the signal I/Q bandwidth. The shape of this Gaussian waveform matches (on average) the OFDM envelope rise and fall time, and this has proven to be equivalent to actually using an "LTE pulse" [28]. Fig. 7 explains this characterization methodology by showing a train of time-delayed Gaussian pulses with amplitude matching the envelope peaks.

This concept is exploited here by using a single Gaussian pulse as the basic waveform to extract the PA gain and current characteristics and map them in terms of coefficients at different temperatures. We note that during characterisation, so that the single Gaussian pulse, itself, does not induce any temperature-based change in characteristics of the RF PA, a short pulse duration (ns $\rightarrow$ μs) should be chosen. This short pulse characterisation can be termed as iso-thermal characterisation of an RF PA [19], [25].

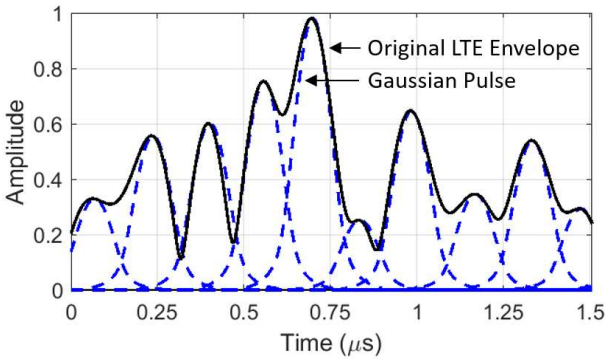

Fig. 7: Study methodology for modulated signals. The envelope of an OFDM signal can be decomposed in a train of amplitude-scaled and time-shifted Gaussian pulses. The peak of each pulse is set to match the local maxima in the envelope while their duration is set to match the LTE pulse width [28].

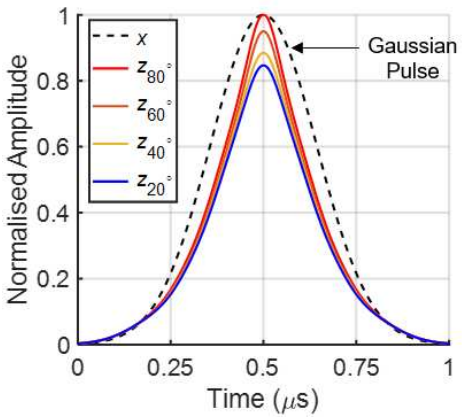

Fig. 8: Different predistorted Gaussian pulses $|z|$ based on the temperature characterisation with a scaling done to achieve a singular gain out of the PA. The PA performs better at cooler temperatures which makes z_{20° smaller than z_{80°, and the characterisation at other temperatures to lie in between these two boundary conditions. $|x|$ is the original Gaussian input used for characterisation at all considered temperatures.

B. DPD Extraction Procedure

As discussed in Section II-D, at least two iso-thermal temperatures, $\theta^*_{j,1} = 20\,^\circ$C and $\theta^*_{j,4} = 80\,^\circ$C, are required for the model. However, for the purpose of validating the linear scaling of the PA characteristics, the following process is repeated also for $\theta^*_{j,2} = 40\,^\circ$C and $\theta^*_{j,3} = 60\,^\circ$C. The procedure is explained as follows:

1) Set the case temperature to m-th value with the TEM chuck regulator. During this, no input is injected to the PA and therefore the channel temperature is iso-thermal with the case temperature[4] (or $\theta^*_{j,m} \cong \theta^*_{c,m}$).
2) A single 1-μs Gaussian pulse is applied to the PA with the baseplate/case temperature set at $\theta^*_{c,m}$. As detailed in Section IV-A the iso-thermal gain $G_{pa}(|x|, \theta^*_{c,m})$ and current $F_{pa}(|x|, \theta^*_{c,m})$ characteristics are extracted.
3) The coefficients $\gamma(\theta^*_{j,m})$ and $\phi(\theta^*_{j,m})$ of the DPD model and PA drain current model are fitted to a polynomial as in (14), (16) by means of least-squares. For this work,

[4]This is because of the class-B operation.

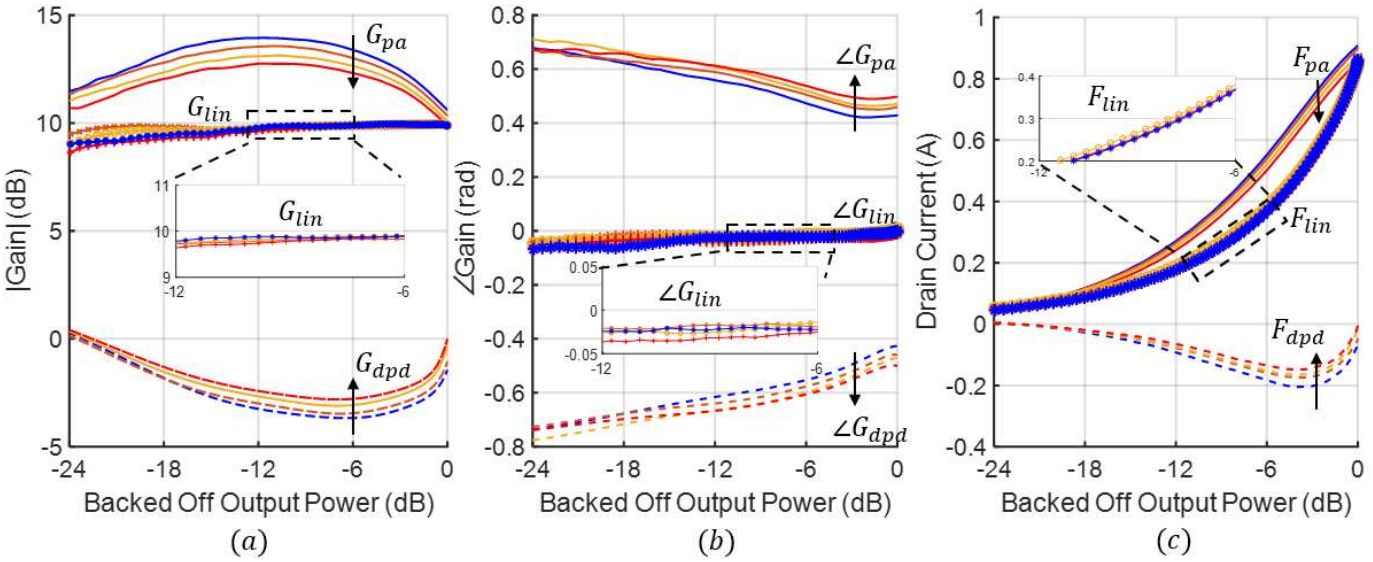

Fig. 9: (a): G_{pa} represents the PA only gain for different temperatures with the arrow indicating a temperature drift from $\theta_C = 20°40°, 60°, 80\,°\text{C}$ and G_{dpd} indicating the gain for the predistorter. G_{lin} is achieved when the PA+DPD is used, for all temperatures within 20° and 80 °C. (b): Indicates the phase offset with similar conditions with the result of all phase cancellations after predistortion, i.e. $\angle G_{pa} + \angle G_{dpd} = \angle G_{lin} = 0(rad)$. (c): Drain current, due to this being a current generator follows the gain characteristics and a singular F_{lin} is achieved for all considered temperatures while the PA only F_{pa} presents a negative thermal coefficient.

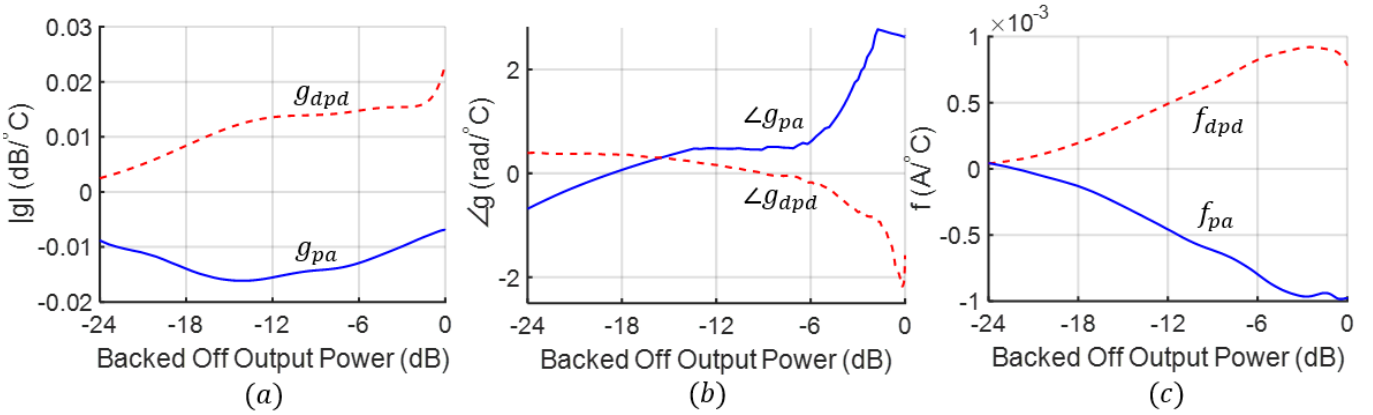

Fig. 10: (a): Sensitivity of the PA gain g_{pa} and of the proposed DPD g_{dpd} from the collected iso-thermal data from 9(a), over the whole temperature range $\Delta\theta = 60\,°\text{C}$. (b): Phase sensitivity calculated from data in Fig 9(b) and (c): PA drain current sensitivity f_{pa} which has a negative thermal coefficient and DPD drain current sensitivity f_{dpd} has a positive thermal coefficient.

the polynomial order was set[5] to $K_G = 9$ for the gain and $K_F = 9$ for the current.

4) The extracted polynomial coefficients at different temperatures are stored for later use.
5) The steps 1) to 4) are eventually repeated for every temperature.

From Section II-D, to achieve a linearized gain G_{lin} independent from the transistor temperature, the following normalization is here introduced. The proposed G_{lin} is the large-signal gain of the PA at the highest temperature ($\theta^*_{j,max} = 80\,°\text{C}$) and maximum input power ($P_{in} = 32\,\text{dBm}$). This scaling is done by normalising the output of the characterisation data at other temperatures ($< 80\,°\text{C}$) by the maximum output power ($P_{o,max} = 42\,\text{dBm}$). These scaled results are then fitted into the same polynomial fitting and a set of DPD coefficients are extracted and the results of which are plotted in Fig. 8. Here, $|x|$ is the original characterisation Gaussian pulse that is injected into the PA at all considered temperatures and $|z|$ is the result after scaling. It is clear that the scaling implemented at 20 °C results in a lower amplitude when compared to 80 °C, which corresponds to the normalization power of $P_{o,max} = 42\,\text{dBm}$ and in this case it reaches a maximum amplitude of 1. For illustration purposes, also the other two temperatures, comprised between the two temperature boundaries (20 ° and 80 °C), are reported on the same plot. If the temperature of the device goes beyond the maximum considered temperature, the amplitude of z will clip to 1. This limitation can be resolved by characterising the PA at even higher temperatures at the expense of a reduction in the linearized gain G_{lin}. A higher linearized gain can

[5]The value of these polynomial orders are chosen by initially setting to a low value of 3 and increasing the factor by 1 till the best response. Having a high polynomial order (>13) has a negative effect on a single pulse characterisation.

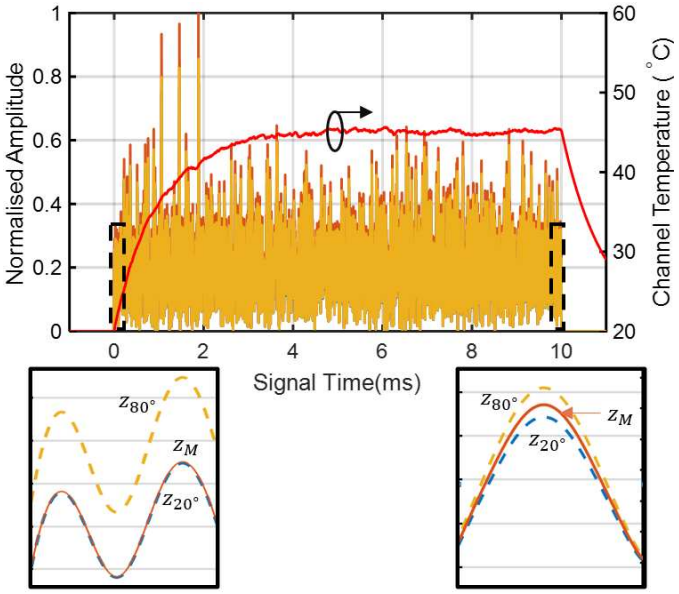

Fig. 11: Validation of the approach, for a 100 kHz signal, with the temperature estimated on the right axis and the amplitude of the distorted signal $z(t)$ on the left. The thermal sensitivity with the temperature information shifts the amplitude of $|z_M|$ from the boundary condition of $|z_{20\circ}|$ at the start of the signal and towards $|z_{80\circ}|$ at the end of the signal. As the temperature estimated is $< 80°$C, the amplitude does not reach $|z_{80\circ}|$.

be instead achieved by reducing the temperature window at lower temperatures which also can be helpful in increasing the reliability of the device.

C. Characterization Results

1) Iso-Thermal Data: Fig. 9 shows the PA and DPD iso-thermal characteristics. Starting from left, G_{pa} is the non-linear PA gain, G_{dpd} is the DPD gain, and $G_{lin} = 9.9$ dB is the gain after linearization, i.e $(G_{pa} + G_{dpd})$ and is the same for all temperatures due to the scaling done in Section IV-B. The amplitude $|G_{pa}|$ differs both in back-off and at large-signal depending on the temperature. Conversely, $|G_{dpd}|$ presents opposite thermal behaviour both in back-off and at large signal.

With regards to the phase offset, $\angle G_{pa}$ tends to increase at increasing temperatures, especially at saturation levels. This behaviour is captured also by the DPD with $\angle G_{dpd}$ but in the opposite fashion. When linearization is applied, the phase difference becomes approximately zero, Fig. 9(b) cancelling any AM/PM non-linearity introduced by the PA for all temperatures.

Like the gain of the PA, the current also follows a negative thermal coefficient, Fig. 9(c). After DPD, the PA is conditioned to have a single gain for all conditions which inherently makes the drain current follow the same path of having a single current profile F_{lin}. We report, F_{dpd} shown in Fig. 9(c), is not a physical quantity that is quantified for this work but just the effect of the DPD on the drain current at every considered temperature to achieve F_{lin}.

2) Temperature Sensitivity: With the aforementioned characteristics, a linear thermal sensitivity for all quantities extracted during the characterisation process are computed

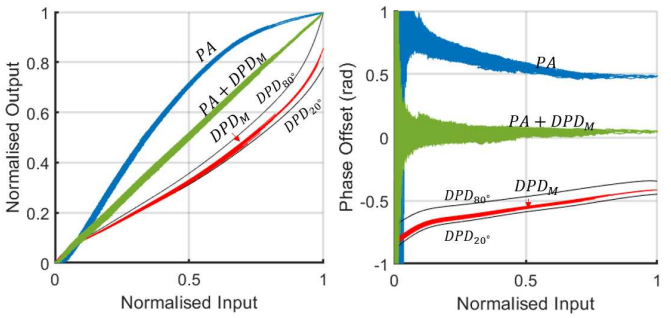

Fig. 12: Dynamic AM/AM and AM/PM validation with PA representing the PA only case, DPD_M representing the modelled DPD, $DPD_{20\circ}$ and $DPD_{80\circ}$ as the iso-thermal characterisations and finally $PA + DPD_M$ as the outcome. With the thermal sensitivity, it is clear that both the amplitude and the phase of DPD_M adapts to signal which can be classified as adding memory to the model for better linearization. With a lower temperature estimation, from Fig. 11, the amplitude and phase of the DPD_M lie between the two boundary conditions.

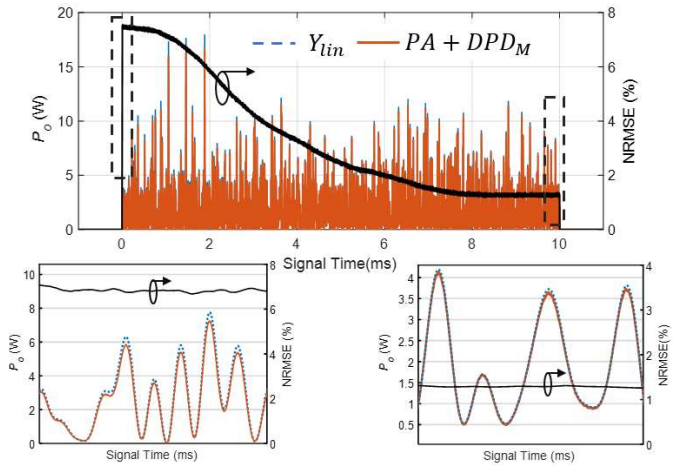

Fig. 13: Validation of the $PA + DPD_M$ output signal to constitute the effectiveness of achieving the proposed G_{lin} and is stable over the whole signal period. For this, an output is created manually, $(y_{lin} = G_{lin} \cdot x)$, with x being the original 100-kHz OFDM signal. An error term is calculated between the two outputs and plotted on the right axis, similar to $|z_M|$ in Fig. 11, the output $PA + DPD_M$ here gradually approaches to y_{lin} levels with the NRMS-Error at the end of the signal $\sim$1%.

and plotted in Fig. 10. For this, the temperatures of the two boundary conditions are chosen and a temperature step ($\Delta\theta = 60\,°$C) is used. We note the PA gain amplitude exhibits a typical thermal sensitivity of -0.15 dB/°C and maximum phase offset of 2 rad/°C over the whole input power range. The DPD sensitivities g_{dpd} and $\angle g_{dpd}$ represent somewhat of an opposite trend. As for the drain current, the thermal sensitivity f_{pa} and f_{dpd} is shown in Fig. 10(c), which reports a total change in current $\cong 1\%$ over the whole temperature range. Thus to simplify the current model the sensitivity was removed and only the iso-thermal data shown in Fig. 9(c) is used.

With the assumption that the majority of the non-linearities introduced in the PA are due to temperature drifts in the channel, we expect that the thermal sensitivities shown in Fig. 10, in conjunction with the temperature information in estimated by the thermal model to add the necessary memory (non-linearity) to this simple iso-thermal characterisation

based DPD approach, reported in (18). Thus, adopting the proposed strategy will reduce the requirement of large number of Look-Up-Tables (LUTs) which are a part of the physical fabric, for lower complexity and power consumption [27].

V. Model Validation

A. Time Domain Analysis

After a preliminary validation of the model, a 100-kHz OFDM signal is considered as the input to the PA. With a time frame of 10-ms and a high PAPR signal (9 dB) the signal-induced temperature within the device should be, moderately low. Fig. 11 shows the whole signal duration, with the start and finish enlarged in the figure inset and the estimated temperature on the right axis. For this test, the temperature of the PA, at the start of the signal, is $\theta_c = 20°$C. A thermal resistance of $R_\theta = 4.3°$C/W and a thermal capacitance $C_\theta = 0.008$ J/°C is considered.

We note very small fluctuations in the temperature estimated for this 100-kHz signal, in Fig. 11, possibly due to the variations in the dissipated power [25]. Both, $|z_{20^\circ}|$ and $|z_{80^\circ}|$ act as the boundary for the proposed $|z_M|$. At the start of the signal, with little or no temperature drift from the set case the amplitude $|z_M|$ matches $|z_{20^\circ}|$ and towards the end of

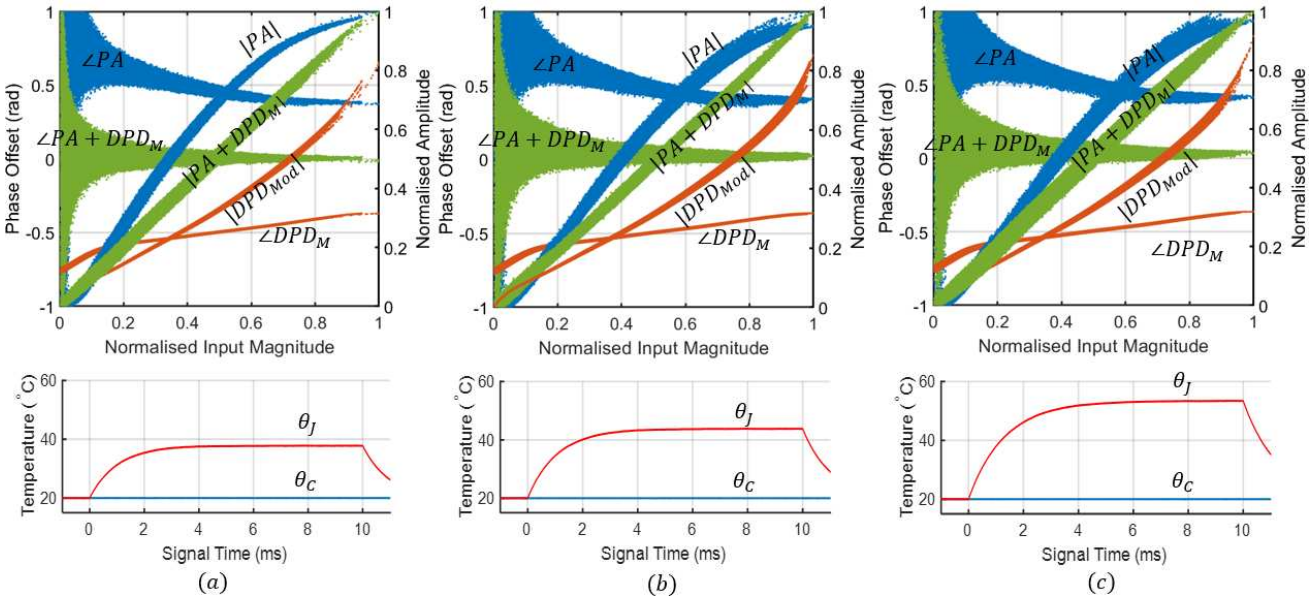

Fig. 14: AM/AM, AM/PM, and channel temperature of the PA, DPD, and PA+DPD. (a): 12-dB PAPR signal, (b): 9-dB PAPR signal, (c): 6-dB PAPR signal. The AM/AM and AM/PM characteristics of the PA (blue) present significant memory effects which result in dispersed characteristics. When DPD is employed (brown), the memory part of the model corrects for them resulting in a less dispersed linearized characteristic (green). The estimated internal temperatures using a single-pole thermal network are also reported to highlight the temperature variation.

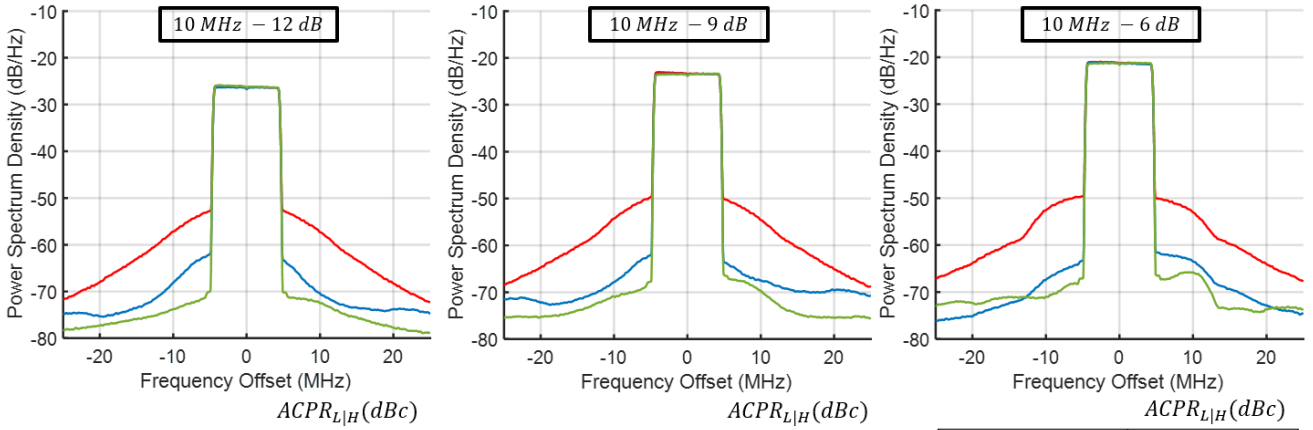

$ACPR_{L|H}(dBc)$

	(a)	(b)	(c)
NO DPD	-27.5 | -27.4	-27.0 | -24.7	-29.3 | -28.7
DPD ISO	-41.3 | -41.1	-43.1 | -44.0	-45.1 | -43.0
DPD MODEL	-45.9 | -45.0	-46.5 | -45.3	-47.5 | -45.6

Fig. 15: PA output spectra of the three different LTE signals, shown in Fig. 14, with only the PA (Red) termed as "NO DPD", with iso-thermal DPD_{80° shown in (Blue) and termed as "DPD ISO" and finally the proposed DPD model (Green) termed as "DPD MODEL". Here, (a) represents the 12-dB case, (b) 9-dB and (c) as the 6-dB. For all different cases, the Adjacent-Channel-Power-Ratio (ACPR) is calculated and reported.

the signal is between the two limits. The drift in this signal amplitude is a result of the temperature change from 20°C to 43 °C, where from the first equation in (18), the sensitivity creates a negative or positive impact on the amplitude and phase of the iso-thermal characterisation. This correction, introduces the memory in z_M that cancels out the PA memory due to temperature effects. This added memory can also be observed in Fig. 12, where for the AM/AM plot, DPD_M is the computed pre-distortion model with highlighted the lower DPD_{20° and higher DPD_{80° temperature boundaries. With the estimated temperature being lower than the maximum ($<$ 80°C), the amplitude of DPD_M does not reach the normalised maximum of 1. This signal when injected into the PA leads to a linearized output $PA + DPD_M$. Similar considerations apply for the phase in the AM/PM whereas the pre-distorted signal phase $\angle z$ is always comprised between the upper and lower boundaries at 20 and 80 °C.

To confirm that this approach reaches the linearised goal of G_{lin} irrespective of the temperature, the output of $PA + DPD_M$ in Watt is compared to a linear output y_{lin}. This output, y_{lin}, is created by manually applying the proposed $G_{lin} = 9.9$ dB to the original input OFDM signal x. The comparison is shown here in terms of a Normalised-Root-Mean-Squared-Error (NRMSE) between the two outputs and is shown in Fig. 13.

B. Multiple PAPRs in Frequency Domain Analysis

From the last section, the impact of the amplitude adjusted $|z_M|$ can be now quantified when the PAPR of a signal is changed, i.e. the input signal is changed, in the PA+DPD system. For this, three different 10-MHz LTE signals with 6-, 9-, and 12 dB PAPRs are considered as input. Here, the initial temperature for all the three cases at which the PA starts at is $\theta_c = 20$ °C and we note that with a lower PAPR, the PA operates "hotter" while for high PAPRs it works in "cooler" conditions, shown at the bottom of Fig. 14. First the non-linear cancellation in terms of the dynamic AM/AM and AM/PM is shown in Fig. 14. The "PA" exhibits significant memory effects, visible dispersed points, especially when the PAPR of the signal is low. This is a clear indication of the temperature induced non-linear memory. "DPD_M" shows the resultant predistortion applied to the PA which adapts to the change of the signal and a linear "$PA+DPD_M$" the resultant output for all the three cases. The amplitude of the DPD_M is dependant, as per the characterisation, on the temperature and for the 6-dB case, is the highest.

Second, Fig. 15 shows the output spectrum of three aforementioned signals. Here the $PA+DPD_M$ is compared to $PA+DPD_{80^\circ}$, which are represented as "DPD MODEL" and "DPD ISO" respectively. To differentiate the two, numerically, the Adjacent-Channel-Power-Ratio (ACPR) of the outputs are reported. In all cases, "DPD MODEL" improves by 3-4 dB at the side bands than the "DPD ISO" approach. This approach, as per dependant on a single temperature characterisation, in this case $\theta_c = 80$°C, and without any temperature sensitivity is similar to $|z_{80^\circ}|$ in the time validation. It is also observed that with an increase of temperature the non-linearities in

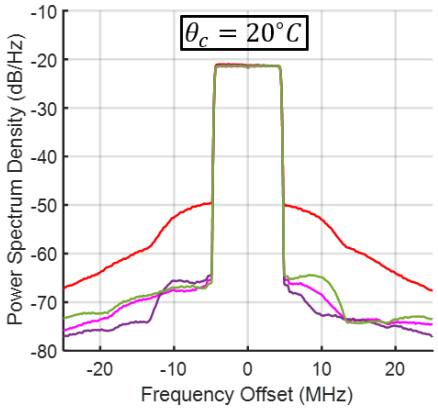

	$ACPR_{L\|H}(dBc)$
NO DPD	-29.3 | -28.9
DPD MP	-46.8 | -46.5
DPD GMP	-46.0 | -47.8
DPD MODEL	-46.4 | -45.0

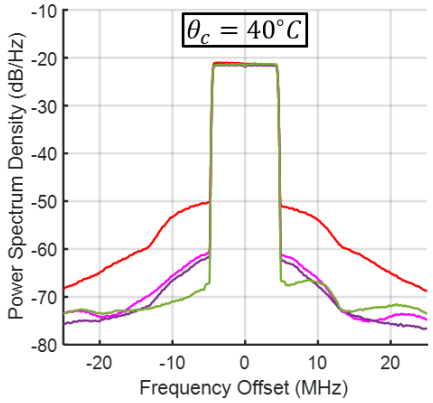

	$ACPR_{L\|H}(dBc)$
NO DPD	-28.9 | -29.5
DPD MP	-38.5 | -38.6
DPD GMP	-38.8 | -39.2
DPD MODEL	-46.1 | -44.8

Fig. 16: (Top): Comparison of the three different DPD models for a 10-MHz 6-dB at $\theta_c = 20$°C, where "DPD MODEL" refers to the proposed model, "DPD MP" refers to a memory-polynomial and "DPD GMP" as Generalised-Memory-Polynomial. Both the MPs are trained in these conditions thus providing a better symmetry in cancellation. (Bottom) when the temperature is changed $\theta_c = 40$°C, the same coefficients extracted before for both MPs fail to match the performance of the proposed model which adapts to the change of the external temperature by sensing the case temperature.

PA, out of the considered band, decrease. The asymmetry, in cancellation, at lower PAPR signals is assumed to be due to other effects (possibly charge trapping) that are not captured by the model. We note, that with lower PAPR signals or higher temperatures, the linearization performance between "DPD ISO" and "DPD MODEL" are closer than in cooler conditions as the temperature approaches 80°C.

C. Comparison with other DPD approaches

Next, to validate the model with other approaches, the same 10-MHz signals were used. A Memory-Polynomial (MP)

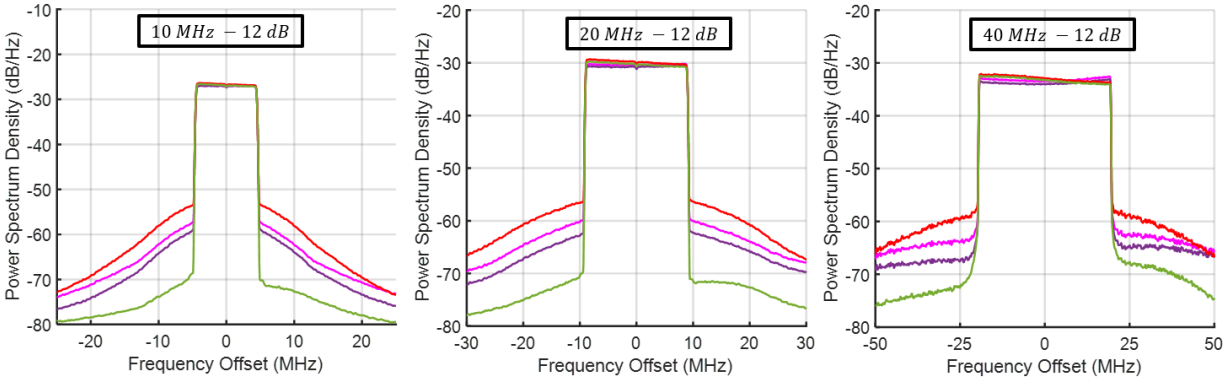

	$ACPR_{L\|H}(dBc)$
NO DPD	-27.9 | -27.5
DPD MP	-31.8 | -31.7
DPD GMP	-33.5 | -33.8
DPD MODEL	-44.4 | -45.0

(a)

	$ACPR_{L\|H}(dBc)$
NO DPD	-28.8 | -28.7
DPD MP	-32.3 | -32.6
DPD GMP	-34.6 | -35.0
DPD MODEL	-44.0 | -42.4

(b)

	$ACPR_{L\|H}(dBc)$
NO DPD	-25.1 | -24.6
DPD MP	-29.3 | -29.4
DPD GMP	-32.2 | -30.1
DPD MODEL	-40.2 | -37.5

(c)

Fig. 17: Comparison for different bandwidths reporting (a) for a 10-MHz, (b) for a 20-MHz and (c) for a 40-MHz signal. Here, the case temperature in all cases is $\theta_c = 20°$C. The proposed model shows a clear advantage over the MP and GMP. Both memory polynomials were trained on an actual LTE signal (10-MHz with 6-dB signal). This clearly shows the need of re-characterisation for these approaches for signal variations, where the proposed model has the ability to adapt to these signal variations for appropriate linearization.

and a Generalised-Memory-Polynomial (GMP) are trained on the signal that induces the highest temperature, 6-dB PAPR signal starting at a case temperature of $\theta_c = 20\,°$C. Both are trained with a polynomial order ($K_{Mp,Gmp} = 9$) and memory ($M_{Mp,Gmp} = 3$), with the added symmetrical lead-lag signal memory tap ($L_{Gmp} = 3$) in the GMP case [29]. The results of these, with the proposed model are reported in Fig. 16 and Fig. 17.

Fig. 16, reports the comparison of the three different approaches when the external (ambient) temperature of the PA is changed. Initially, in Fig. 16(Top) with similar conditions to when characterising for both MP and GMP, the cancellation for all approaches is similar. A better symmetry is seen, for the two memory polynomials, as the training on the actual signal gives the advantage to capture other effects that the proposed model does not consider. But when the ambient temperature is changed, reported in Fig. 16(Bottom), the same MP and GMP coefficients fail to provide the same effective linearization as the proposed model reports. This clearly shows that these conventional approaches need a coefficient update to be effective over a wide temperature range while the model, because of the case temperature sensing and thermal network, has the ability to predict the current channel temperature.

Usually, a DPD coefficient update requires the PA output to be sensed, downconverted, digitized, and a large matrix inverted. This entails a significant power consumption (at least in terms of ADCs) with a marginal improvement of the total system linearity, especially if the re-characterisation has to be done for a small change of the ambient/case temperature. By having the low-frequency temperature feedback the need of such a complex system can be reduced as this feedback can be directly implemented on the FPGA and does not require any processing, thus reducing the hardware complexity and power consumption.

Finally, Fig. 17 shows the spectra without and with MP, GMP, and presented DPD. For a fair comparison, the case temperature and the signal PAPR (12-dB) of the different signals is the same. With such a high PAPR, the PA works in a relatively cooler condition. This cooler condition has a negative effect when using the coefficients extracted at higher temperature conditions, or vice-versa. Even at higher bandwidths, the model is capable of linearizing the PA as can be seen in Fig. 17(a)-(c). We note, at higher bandwidths (20- and 40-MHz) there is an increase of asymmetry in the cancellation with this DPD, and this is due to the modelling specific to temperature related effects and not for faster effects such as bias-network dispersion which becomes an even bigger issue as the bandwidth of the signal increases [30].

These measurements, clearly indicate that the memory introduced in the characterisation procedure of the MP and GMP predistortion limits their capabilities with a signal induced temperature which constantly changes. With this, we can term them as signal dependant approaches. The proposed approach, due to its instrinsic level characterisation is true for a longer period of time unless the device is severely damaged due to reliability issues or ageing. While ageing is random and difficult to predict, reliability issues due to thermal stress can be minimized which gives great advantage to this approach with the knowledge of the instantaneous temperature.

VI. Conclusion

This work presents a digital pre-distortion (DPD) capable of compensating memory effects in a non-linear RF power amplifier (PA). This DPD provides a linearized gain with a fixed gain value of $G_{lin} = 10$ dB despite the temperature variation in the device due to self-heating or ambient temperature changes. The proposed DPD uses a Gaussian pulse characterisation to extract the PA response at different

temperatures. A thermal network is employed to calculate the channel temperature based on measuring the case temperature of the device. This temperature information helps the model to adjust the coefficients based on the instantanous channel temperature. The robustness of this model is demonstrated by considering a wide temperature range from 20° to 80°C and varying signal peak-to-average power ratios (PAPRs) from 6 to 12 dB. First, the normalized root mean square error (NRMSE) is calculated to show the efficacy of the model to achieve G_{lin} despite the signal induced memory effects, and a value below 7% is achieved. Second, the linearization performance for a PAPR equal to 12, 9, and 6 are evaluated in terms of adjacent channel power ratio (ACPR) with improvements between 1 and 4 dB as compared to the temperature-less DPD model. At last, the presented DPD is compared with other approaches such as memory polynomial and generalized memory polynomials to show how the presented DPD is capable of adapting while the others need a re-calculation of the coefficients from a new set of I/Q data.

ACKNOWLEDGMENTS

The authors would like to thank Prof. Peter Crook from the University of Bristol with the setup help, Toshiba Europe Ltd. for the support in fabrication and funding.

REFERENCES

[1] J. J. Komiak, "Gan hemt: Dominant force in high-frequency solid-state power amplifiers," *IEEE Microwave Magazine*, vol. 16, no. 3, pp. 97–105, 2015.

[2] A. Prejs, S. Wood, R. Pengelly, and W. Pribble, "Thermal analysis and its application to high power gan hemt amplifiers," in *2009 IEEE MTT-S International Microwave Symposium Digest*, 2009, pp. 917–920.

[3] C. Florian, T. Cappello, A. Santarelli, D. Niessen, F. Filicori, and Z. Popović, "A prepulsing technique for the characterization of gan power amplifiers with dynamic supply under controlled thermal and trapping states," *IEEE Transactions on Microwave Theory and Techniques*, vol. 65, no. 12, pp. 5046–5062, 2017.

[4] T. Cappello, A. Santarelli, and C. Florian, "Dynamic ron characterization technique for the evaluation of thermal and off-state voltage stress of gan switches," *IEEE Transactions on Power Electronics*, vol. 33, no. 4, pp. 3386–3398, 2018.

[5] R. Mohan, Undeland, *Power Electronics / Converters, Applications, and Design 2nd edition*, 2nd ed. John Wiley & Sons, 1995, ch. 29.

[6] U. K. Mishra, L. Shen, T. E. Kazior, and Y.-F. Wu, "Gan-based rf power devices and amplifiers," *Proceedings of the IEEE*, vol. 96, no. 2, pp. 287–305, 2008.

[7] B. Green, K. Moore, D. Hill, M. CdeBaca, and J. Schultz, "Gan rf device technology and applications, present and future," in *2013 IEEE Bipolar/BiCMOS Circuits and Technology Meeting (BCTM)*, 2013, pp. 101–106.

[8] D. Maier, M. Alomari, N. Grandjean, J.-F. Carlin, M.-A. Diforte-Poisson, C. Dua, A. Chuvilin, D. Troadec, C. Gaquière, U. Kaiser, S. L. Delage, and E. Kohn, "Testing the temperature limits of gan-based hemt devices," *IEEE Transactions on Device and Materials Reliability*, vol. 10, no. 4, pp. 427–436, 2010.

[9] G. Crupi, A. Raffo, G. Avolio, D. M. M.-P. Schreurs, G. Vannini, and A. Caddemi, "Temperature influence on gan hemt equivalent circuit," *IEEE Microwave and Wireless Components Letters*, vol. 26, no. 10, pp. 813–815, 2016.

[10] C. Florian, A. Santarelli, R. Cignani, and F. Filicori, "Characterization of the nonlinear thermal resistance and pulsed thermal dynamic behavior of algan–gan hemts on sic," *IEEE Transactions on Microwave Theory and Techniques*, vol. 61, no. 5, pp. 1879–1891, 2013.

[11] T. Cappello, A. Santarelli, and C. Florian, "Dynamic ron characterization technique for the evaluation of thermal and off-state voltage stress of gan switches," *IEEE Transactions on Power Electronics*, vol. 33, no. 4, pp. 3386–3398, 2018.

[12] D. Kim and S. An, "Experimental analysis of papr reduction technique using hybrid peak windowing in lte system," *EURASIP Journal on Wireless Communications and Networking*, vol. 2015, 12 2015.

[13] "GaN Thermal Analysis for High-Performance Systems," https://www.qorvo.com/resources/d/qorvo-gan-thermal-analysis-for -high-performance-systems-white-paper, accessed: 2021-07-12.

[14] M. Kuball, G. J. Riedel, J. W. Pomeroy, A. Sarua, M. J. Uren, T. Martin, K. P. Hilton, J. O. Maclean, and D. J. Wallis, "Time-resolved temperature measurement of algan/gan electronic devices using micro-raman spectroscopy," *IEEE Electron Device Letters*, vol. 28, no. 2, pp. 86–89, 2007.

[15] S. Boumaiza and F. Ghannouchi, "Thermal memory effects modeling and compensation in rf power amplifiers and predistortion linearizers," *IEEE Transactions on Microwave Theory and Techniques*, vol. 51, no. 12, pp. 2427–2433, 2003.

[16] J. Mazeau, R. Sommet, D. Caban-Chastas, E. Gatard, R. Quere, and Y. Mancuso, "Behavioral thermal modeling for microwave power amplifier design," *IEEE Transactions on Microwave Theory and Techniques*, vol. 55, no. 11, pp. 2290–2297, 2007.

[17] Y. Zhu, J. Twynam, M. Yagura, M. Hasegawa, T. Hasegawa, Y. Eguchi, A. Yamada, E. Suematsu, K. Sakuno, H. Sato, and N. Hashizume, "Analytical model for electrical and thermal transients of self-heating semiconductor devices," *IEEE Transactions on Microwave Theory and Techniques*, vol. 46, no. 12, pp. 2258–2263, 1998.

[18] G. P. Gibiino, T. Cappello, D. Niessen, D. M. M.-P. Schreurs, A. Santarelli, and F. Filicori, "An empirical behavioral model for rf pas including self-heating," in *2015 Integrated Nonlinear Microwave and Millimetre-wave Circuits Workshop (INMMiC)*, 2015, pp. 1–3.

[19] G. Jindal, G. Watkins, K. Morris, and T. Cappello, "An rf power amplifier behavioural model with low-complexity temperature feedback for transmitter arrays," in *Presented at 2021 IEEE MTT-S International Microwave Symposium (IMS)*, 2021.

[20] J. Wood, *Behavioral Modeling & Linearization of RF Power Amplifiers*, 1st ed. Artech House, Boston, 2014, ch. 8.

[21] Y.-J. Liu, J. Zhou, W. Chen, and B.-H. Zhou, "A robust augmented complexity-reduced generalized memory polynomial for wideband rf power amplifiers," *IEEE Transactions on Industrial Electronics*, vol. 61, no. 5, pp. 2389–2401, 2014.

[22] F. M. Barradas, L. C. Nunes, T. R. Cunha, P. M. Lavrador, P. M. Cabral, and J. C. Pedro, "Compensation of long-term memory effects on gan hemt-based power amplifiers," *IEEE Transactions on Microwave Theory and Techniques*, vol. 65, no. 9, pp. 3379–3388, 2017.

[23] T. Gotthans, R. Marsalek, and J. Gotthans, "Temperature compensation-based behavioral modeling for digital predistortion of rf power amplifiers," in *2019 IEEE International Symposium on Signal Processing and Information Technology (ISSPIT)*, 2019, pp. 1–4.

[24] P. M. Tomé, F. M. Barradas, T. R. Cunha, and J. C. Pedro, "A multiple-time-scale analog circuit for the compensation of long-term memory effects in gan hemt-based power amplifiers," *IEEE Transactions on Microwave Theory and Techniques*, vol. 68, no. 9, pp. 3709–3723, 2020.

[25] G. Jindal, J. Pomeroy, G. Watkins, K. Morris, M. Kuball, and T. Cappello., "High-speed electro-thermal measurements in rf power amplifiers using thermo-reflectance," *International Workshop on Integrated Nonlinear Microwave and Millimetre-wave Circuits (iNMMiC)*, 2022.

[26] K. R. Bagnall and E. N. Wang, "Transient thermal dynamics of gan hemts," in *2016 15th IEEE Intersociety Conference on Thermal and Thermomechanical Phenomena in Electronic Systems (ITherm)*, 2016, pp. 1551–1557.

[27] T. Cappello, G. Jindal, J. Yanez, and K. Morris, "Power consumption and linearization performance of a bit- and frequency-scalable am/am am/pm pre-distortion on fpga," *International Workshop on Integrated Nonlinear Microwave and Millimetre-wave Circuits (iNMMiC)*, 2022.

[28] T. Cappello, Z. Popovic, K. Morris, and A. Cappello, "Gaussian pulse characterization of rf power amplifiers," *IEEE Microwave and Wireless Components Letters*, pp. 1–4, 2021.

[29] D. Morgan, Z. Ma, J. Kim, M. Zierdt, and J. Pastalan, "A generalized memory polynomial model for digital predistortion of rf power amplifiers," *IEEE Transactions on Signal Processing*, vol. 54, no. 10, pp. 3852–3860, 2006.

[30] S. Jin, B. Park, K. Moon, M. Kwon, and B. Kim, "Linearization of cmos cascode power amplifiers through adaptive bias control," *IEEE Transactions on Microwave Theory and Techniques*, vol. 61, no. 12, pp. 4534–4543, 2013.

Gautam Jindal received his B.Eng (with Honors) in Electrical and Electronic Engineering from University of Bristol in 2018 and is currently pursuing a Ph.D. degree at the Communications Systems and Networking lab at the University of Bristol funded by Toshiba Research Europe Ltd. His current research lies in Low Complexity Digital-Pre-distortion (DPD) for RF Amplifiers and is looking to solve temperature related issues. His interest lie in non-linear RF device modelling, GaN transistors, reliability concerns and linearization.

Gavin T. Watkins is a member of both the Institute of Engineering Technology (IET) and the European Microwave Association. He received the MEng degree in Electrical and Electronic Engineering in 2000 from the University of Bristol and a PhD from the same institution in 2003 on the topic of Wideband Feedforward Amplifiers for Software defined Radios. In 2008 he joined Toshiba Research Europe Limited where he is currently the lead for the Analogue and Digital Systems Programme. He is also the vice chair for the IET RF and Microwave Technical Network and is a regular IET and IEEE reviewer. His research interests include linear power amplifiers, high efficiency system architectures, analogue circuitry, active gate drivers for power electronics, device characterization, 3D printing for RF and Full Duplex communications systems.

Kevin Morris received the B.Eng. and Ph.D. degrees in electronics and communications engineering from the University of Bristol, Bristol, U.K., in 1995 and 1999 respectively. He currently is a full professor and heads the CSN research group in the Department of Electrical and Electronic Engineering, University of Bristol. Currently, he is involved with a number of research programs within the U.K. He has authored or co-authored 100 academic papers and is the joint author of five patents. His research interests are principally in looking at methods of reducing power consumption in communications systems, including the area of radio frequency hardware design with specific interest in the design of efficient linear broadband power amplifiers for use within future communications systems

Tommaso A. Cappello (S'13–M'17) received the Laurea degree (cum laude) in electrical engineering and the Ph.D. degree from the University of Bologna, Italy, in 2013 and 2017, respectively. Between 2017 and 2019, he was a Post-doctoral Research Associate with the Microwave and RF Research Group at the University of Colorado Boulder, CO, USA. Since 2020, he is a Lecturer in Electrical and Communication engineering at the University of Bristol, UK. His current research interests include design and characterization of RF and power electronic circuits.